International Journal of Engineering and Science Invention (IJESI)
ISSN (Online): 2319-6734, ISSN (Print): 2319-6726
www.ijesi.org ||Volume 12 Issue 9 September 2023 || PP 38-48

On Silt Fraction Content in Sandy Soils in Context of Permeability Estimation: From Direct Testing To Microstructural Analysis

Maciej Sobótka[1], Bartłomiej Bodak[1]
[1]*Faculty of Civil Engineering, WrocławUniversity of Science and Technology, Poland*

ABSTRACT:*This study investigates the impact of silt fraction content on the permeability of sandy soils. Three distinct sand samples underwent comprehensive laboratory assessments, including granulometric analysis, determination of selected physical properties, and hydraulic conductivity measurements. Subsequently, the soil specimens underwent a sieving process using a 63 μm mesh sieve to eliminate silt particles. All aforementioned examinations were then repeated. Simultaneously, micro-computerized X-ray tomography was utilized to acquire three-dimensional images of the soil microstructure, which were subsequently used to assess permeability. In this context, the granulometric composition was assessed through simulated sifting and hydraulic conductivity was calculated using the Kozeny-Carman equation. Additionally, pore-network modeling and the Lattice-Boltzmann method were employed to achieve the same objective. Following the image processing that involved the removal of particles smaller than 63 μm, the determination of hydraulic conductivity was reiterated. The analyses conducted, along with the comparison of results between the original sands and those devoid of silt fraction, have led to the following key findings: A relatively small silt fraction, even in the order of a few percentage points, can exert a substantial influence on the permeability of sandy soils. The presence of silt content may lead to a noticeable underestimation of permeability values in permeameter tests. Conversely, microstructure-based approaches tend to yield upper bound. Thus, for practical applications, such as numerical simulations, it is advisable to consider these two concurrent approaches as providing lower and upper estimates for permeability in order to obtain a more comprehensive understanding of the fluid flow through sandy soils.*

KEYWORDS: *hydraulic conductivity, micro-tomography, permeability, silt content, soil microstructure*

Date of Submission: 14-09-2023 Date of Acceptance: 29-09-2023

I. INTRODUCTION

Soil permeability plays a crucial role in various aspects of geotechnical engineering and environmental science. It is a fundamental quantity in modelling of fluid flow through porous media that impacts a wide range of applications, from groundwater flow prediction to the design of geotechnical structures. In the realm of geotechnical problems involving poromechanical effects, the accurate prediction of its value significantly impacts the results of numerical simulations involving consolidation, drainage, and response to stress and deformation of the soil subjected to groundwater filtration. In contrast to many purely mechanical properties that can be estimated or measured with a high level of confidence, predicting permeability is a complex undertaking, as it is a function of multiple interrelated parameters rather than a standalone property [1]. These parameters include, but are not limited to, porosity, elongation of flow paths through the pore space, properties of the soil-fluid interface and the distribution of pore sizes within the medium [2].

Permeability is often used interchangeably with the concept of hydraulic conductivity, which takes into account the properties of the migrating fluid, specifically its viscosity, in addition to the microstructural properties of the medium. Those values form the proportionality coefficient of the Darcy equation, which is the fundamental model of laminar viscous flow in porous media [3].

Multiple and diverse approaches have been proposed to predict the permeability of soils, each having some advantages and limitations. If allowed by the construction site conditions, on-site tests have been known to offer reliable outcomes, but often at the expense of high measurement complexity and low spatial resolution of the results. However, this approach is often limited to the subsurface layer of the soil and practically rules out the possibility of assessment at greater depths. Laboratory-based tests on the material extracted from boreholes do not manifest such issues, but are commonly known to be time consuming and require specialized equipment. Therefore, several correlations have been developed that enable estimating permeability from the results of

granulometric analysis, which is one of the basic laboratory-made assessments of soil properties, but with variable credibility of the resulting values [4], [5].

Image-based predictions rely on the real microstructure of the analyzed specimens and, thus, seem to offer deeper insight into the hydraulic properties of soils. Utilizing micro-tomography (micro-CT) scans, certain microstructural parameters that affect permeability can be computed, or fluid flow can be directly simulated through computational fluid dynamics (CFD) methods [6]–[8]. However, these approaches require careful consideration of some of the factors that influence the flow in real granular porous media, but are either not prominent in image-based methods or completely ignored. One such influential factor is the presence of fine particles, specifically the silt fraction and smaller, and their role in the reliability of permeability estimation, both in laboratory and microstructure-based approaches. As it emerges from the present study, even though in some coarser sands these fine particles may constitute less than 5% of the total grain mass, their influence is significant and can result in either underestimation (in permeameter tests) or overestimation (in image-based methods) of soil conductivity.

This study discusses the impact of the silt fraction on the accuracy of permeability estimation for different sands, using a variety of methods. In the following section, the parameters of the samples under consideration, the description of the laboratory measurement methodology, the empirical relations, and their respective results are presented. The third section provides details on the scanning and data preparation process, along with the methodology and results of image-based techniques utilized in the study. The discussion of the methodologies employed forms the fourth section, while the last section summarizes the outcomes and draws conclusions from the study.

II. DIRECT LABORATORY TESTING AND EMPIRICAL CORRELATIONS

In the study three types of sand with diverse characteristics were subjected to testing. Sample 1 (S1) was classified as fine sand, exhibiting a uniform grain size distribution. Sample 2 (S2) represented fine sand as well, but contained a higher overall silt fraction content. Sample 3 (S3) exhibited a broader grain size distribution and was classified as medium sand. Despite varying silt content (≈1% for S1, 10.5% for S2 and <0.8% for S3), none of the samples could be classified as silty sand under European nomenclature.

For each sample, a set of basic laboratory tests was conducted, including granulometric analysis. The results are provided in Table 1. The same samples were later subjected to rinsing in order to remove silt fraction from the soil. The sieve used had a mesh diameter of 63μm. The comparison of grain size distribution curves before and after silt removal is depicted in Fig. 1.

Table 1 Measured properties of the samples

Sample no.	Sample name	Soil type	Bulk density	Specific density	Porosity in loose state	Uniformity coefficient
		[-]	ρ [g/cm^3]	ρ_s [g/cm^3]	φ [-]	U [-]
S1	*fine sand*	*FSa*	*1.54*	*2.63*	*0.41*	*1.840*
S2	*fine sand*	*FSa*	*1.23*	*2.64*	*0.53*	*2.532*
S3	*medium sand*	*MSa*	*1.65*	*2.65*	*0.38*	*3.147*

2.1 Measurements in permeameter

To ensure representative comparison between laboratory and micro-tomography based techniques, the permeameter used in study was custom designed by the authors. The permeameter fixture was a 3D printed part that was used to measure the permeability in the falling head test and accommodate the sample for X-ray micro-computerized tomography (micro-CT) imaging. This ensured that the microstructure of the soil did not change between these two approaches and made it possible to lessen the influence of the scale effect associated with discrepancies in the sample sizes.

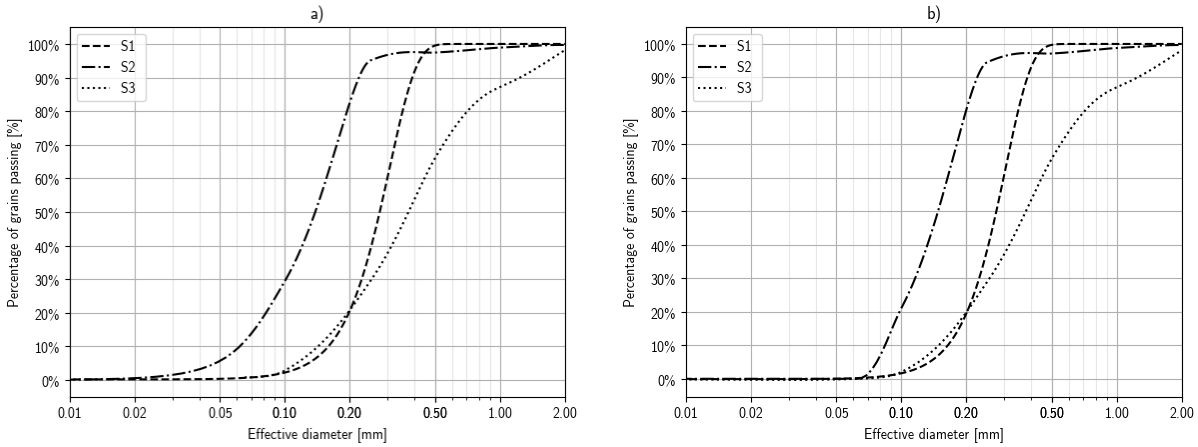

Figure 1 Grain size distribution (GSD) curves: a) before and b) after removal of the silt fraction

During testing, the soil was subjected to the flow of water in a falling-head measurement. The changes in fluid level in time were recorded and later used to fit a theoretical curve with the following equation (1):

$$H(t) = H_0 \cdot exp(-K \cdot \frac{A}{a \cdot L} \cdot (t - t_0)) \quad (1)$$

Here, H(t) denotes the function of the hydraulic height in time, H_0 is the hydraulic height at the start of the test [m], K is the hydraulic conductivity of the sample [m/s], A is the cross-section area of the sample [m^2], L is the length of the sample [m], a is the cross-section area of the measurement pipe [m^2] and t_0 is the parameter corresponding to the start time of the test [s]. The resulting curves were presented in Fig. 2.

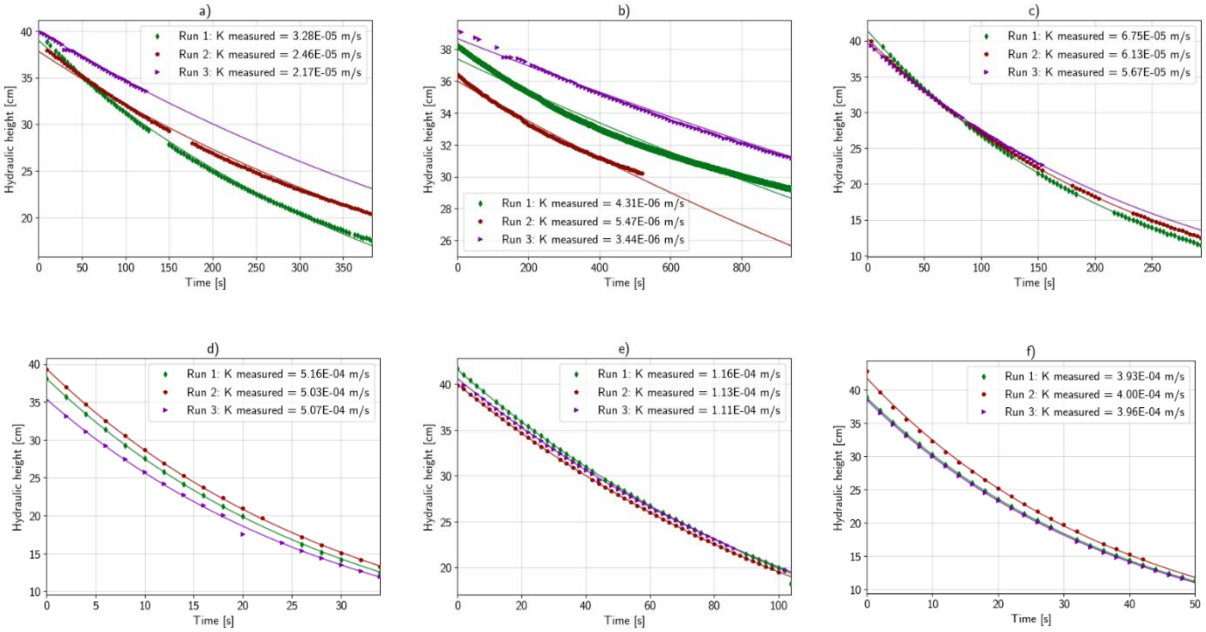

Figure 2 Results of the measurement in permeameter: a), b) and c) original samples S1, S2 and S3, respectively;d), e) and f) rinsed samples S1, S2 and S3 after removal of the silt fraction

The resulting hydraulic conductivity values derived from the curves were later subjected to correction in order to account for the resistance of the permeameter itself and recalculated into hydraulic conductivity at 10°C. The results have been presented in Table 2.

Table 2 Comparison of hydraulic conductivity of original and rinsed samples acquired during tests in permeameter

Sample no.	Sample name		Measured conductivity	Corrected conductivity	Conductivity at 10°C
			K_{meas}[m/s]	K_{corr} [m/s]	$K_{10°C}$ [m/s]
S1	*fine sand*	*original*	*2.63E-5*	*2.68E-5*	*1.96E-5*
		rinsed	*5.09E-4*	*5.56E-4*	*4.17E-4*
S2	*fine sand*	*original*	*4.46E-6*	*4.46E-6*	*3.25E-6*
		rinsed	*1.13E-4*	*1.15E-4*	*8.66E-5*
S3	*medium sand*	*original*	*6.18E-5*	*6.27E-5*	*4.56E-5*
		rinsed	*3.96E-4*	*4.24E-4*	*3.18E-4*

2.2 Estimation using empirical formulae

Empirically-derived formulae provide an accessible method for permeability estimation in cases, where the known properties of the soil are limited to outcomes of granulometric analysis. Those functions correlate the permeability of the soil with the effective diameters of soil particles, defined as the n-th percentile of smallest grain sizes in composition, and in some cases other parameters as well [9]. In the study, the prediction of hydraulic conductivity was conducted with the formulae developed by: Sauerbrey [10], Seelheim[11], Hazen [12], Beyer [13] and United States Bureau of Reclamation (USBR) [14]. The equations, their parameters and general applicability limits were presented in Table 3. The form of the equations was standardized as mentioned by Říha et al. [9].

Table 3 Forms of empirical equations used in the study

Equation name	Equation form	Limits of usage
Sauerbrey	$K = \frac{g}{\nu} \cdot (3.75 \cdot 10^{-3}) \cdot \frac{\varphi^3}{(1-\varphi)^2} \cdot (d_{17})^2$	d_{17}<5mm
Seelheim	$K = 3570 \cdot (d_{50})^2$	*sands and clays*
Hazen	$K = \frac{g}{\nu} \cdot (6 \cdot 10^{-4}) \cdot (1 + 10 \cdot (\varphi - 0.26)) \cdot (d_{10})^2$	d_{10}<3mm d_{10}>0.1mm
Beyer	$K = \frac{g}{\nu} \cdot (6 \cdot 10^{-4}) \cdot \log\left(\frac{500}{U}\right) \cdot (d_{10})^2$	1<U<20 d_{10}<0.6mm d_{10}>60μm
USBR	$K = \frac{g}{\nu} \cdot (4.8 \cdot 10^{-4}) \cdot (1000 \cdot d_{20})^{0.3} \cdot (d_{20})^2$	U<5

In the equations, K corresponds to the hydraulic conductivity in [m/s], g is the gravitational acceleration [m/s^2], ν is the kinematic viscosity [m^2/s], φ is the porosity [-], U is the uniformity coefficient [-] and d_n is the effective diameter of the n-th percentile of the smallest grains [m]. The results of estimation using mentioned equations for the original and rinsed samples were shown in Table 4.

III. IMAGE-BASED ANALYSIS

As mentioned, the same samples were subjected to micro-CT imaging as in the case of tests in permeameter. Therefore, the test results obtained using different approaches concern exactly the same material. Scanning of the samples was performed in the Bruker Skyscan 1172 device. The reconstruction of three-dimensional morphology models was performed using the Feldkamp algorithm [15] in the Bruker NRecon program. The same set of scanning and reconstruction parameters was used for all three samples S1, S2 and S3. These parameters are summarized in Table 5. Figure 3 shows the general view of reconstructed 3D images of the samples analyzed in the study.

Table 4 Results of estimation from empirical formulae

Sample no.	Sample name		Effective diameter d_{17}	Conductivity at 10°C Sauerbrey eq.	Effective diameter d_{50}	Conductivity at 10°C Seelheim eq.	Effective diameter d_{10}	Conductivity at 10°C Hazen eq.	Conductivity at 10°C Beyer eq.	Effective diameter d_{20}	Conductivity at 10°C USBR eq.
			[mm]	*[m/s]*	*[mm]*	*[m/s]*	*[mm]*	*[m/s]*	*[m/s]*	*[mm]*	*[m/s]*
S1	*fine sand*	*original*	*0.189*	*1.223E-04*	*0.277*	*2.747E-04*	*0.161*	*2.413E-04*	*6.579E-04*	*0.197*	*8.664E-05*
		rinsed	*0.193*	*1.290E-04*	*0.277*	*2.747E-04*	*0.165*	*2.547E-04*	*6.957E-04*	*0.201*	*9.074E-05*
S2	*fine sand*	*original*	*0.077*	*9.390E-05*	*0.137*	*6.721E-05*	*0.061*	*5.931E-05*	*8.904E-05*	*0.081*	*1.122E-05*
		rinsed	*0.093*	*1.384E-04*	*0.149*	*7.949E-05*	*0.085*	*1.155E-04*	*1.821E-04*	*0.097*	*1.698E-05*
S3	*medium sand*	*original*	*0.181*	*5.746E-05*	*0.378*	*5.089E-04*	*0.141*	*1.345E-04*	*4.573E-04*	*0.197*	*8.664E-05*
		rinsed	*0.185*	*6.155E-05*	*0.378*	*5.089E-04*	*0.149*	*1.522E-04*	*5.153E-04*	*0.201*	*9.074E-05*

Quantitative analyzes were performed based on binary images of the pore space, limited to cubic volume of interest (VOI), contained entirely within the scanned samples (Fig. 4). The size of the VOI was 400^3px each time. Binarization of the reconstructed sample images was performed using the Otsu algorithm for individual horizontal sections.

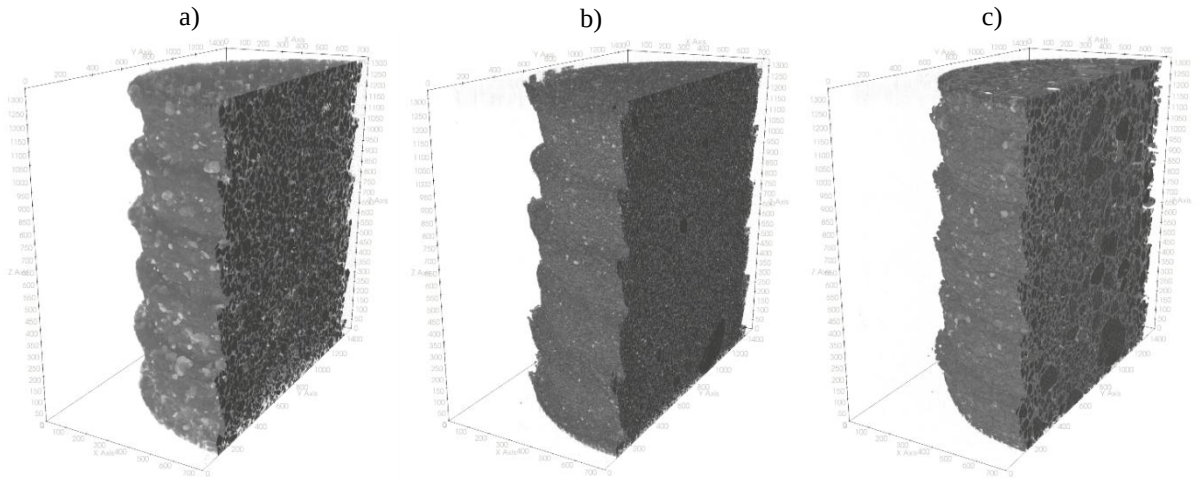

Figure 3 3D rendered views of imaged samples: a) S1, b) S2, c) S3

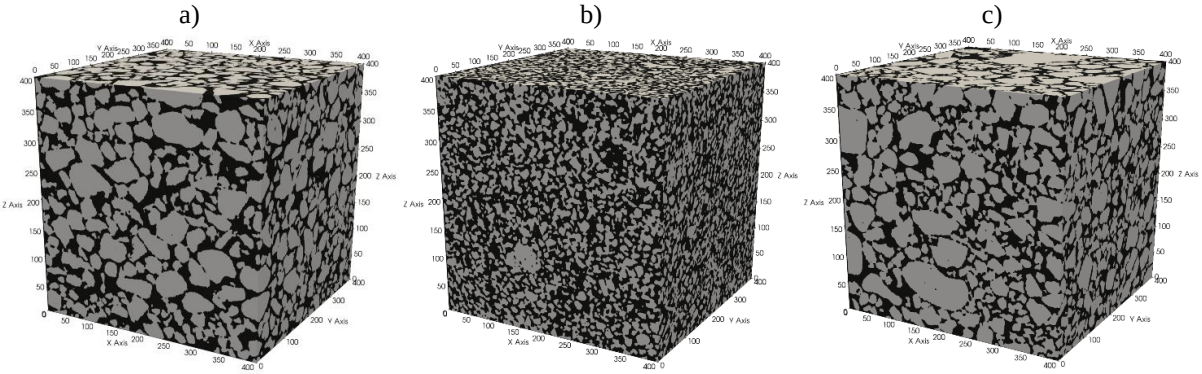

Figure 4 Binary images of pore space limited to cubic VOI: a) S1, b) S2, c) S3

3.1 Simulated sifting

Granulometric analysis is a versatile tool for characterization of grain properties and forms the foundation for correlative methods used to determine various quantities for samples subjected to laboratory measurements. Similarly, simulated sifting enables the characterization of properties of digitized soil scans.

For each segmented region within the 3D image, geometrical properties were computed along with the minimal sieve size required for each grain to pass through. This was accomplished by determining the minimal cuboids circumscribed around the regions. The resulting cumulative distributions of effective diameters, recognized as the second shortest edges of the bounding boxes, closely resemble grain size distribution (GSD) curves obtained through granulometric analysis.

Table 5 Scanning and reconstruction parameters

Parameter	Value
X-ray tube voltage	*80 kV*
X-ray tube current	*126 μA*
Filter used	*Al 0.5 mm*
Angular step	*0.24°*
Resolution	*7.8492 μm*
Smoothing	*1.0*
Ring correction	*10*
Beam hardening correction	*30%*

Those simulated curves served two essential purposes. Firstly, the results of the simulated sifting may serve as a substitute of GSD curves derived from laboratory measurements and as demonstrated in the assessed samples, they exhibited a high level of alignment with the laboratory results. Secondly, the fine particles were removed from the images to get rid of fine soil fraction, similarly as rinsing in the laboratory tests. In this process, every voxel belonging to the grain regions with an effective diameter smaller than the silt particle size limit (63μm) was substituted with pore space. This provided 3D microstructure representations to further compare the original data with that containing no silty fraction.

3.2 Kozeny-Carman equation

Within the spectrum of microstructure-based methods, Kozeny-Carman (K-C) type equations [16]–[18] stand out for their ability to estimate permeability without the need for computationally expensive CFD simulations, while simultaneously incorporating properties of the actual porous medium microstructure more comprehensively than simple correlative relations. The exact form of the equation (2) used in the study is based on the model of flow around submerged particles with notion of hydraulic radius, as presented by Dullien[19]:

$$k = \frac{\varphi}{16(k_0 \cdot \tau)} \cdot \left(\frac{4\varphi}{S \cdot (1-\varphi)}\right)^2 \tag{2}$$

where k stands for the permeability of the medium [m^2], k_0 is a constant with a value of 2.0~2.5 [20], φ is the porosity of the medium, τ is the tortuosity of the pore space and S is the specific surface area of the medium per unit volume [1/m]. Tortuosity of the samples was computed numerically with the PyTrax algorithm [21], while the specific surface area was obtained with the help of algorithms contained in PoreSpy framework [22]. As mentioned, calculations were conducted twice – for the original samples and samples after virtual silt removal. The outcomes of this procedure were summarized in Table 6.

Table 6 Results of estimation using Kozeny-Carman equation

Sample		Porosity dervied from 3D image	Tortuosity	Specific surface area	Conductivity at 10°C
		φ [-]	*τ [-]*	*S [1/m]*	*$K_{10°C}$ [m/s]*
S1	*original*	*0.365*	*1.847*	*38748*	*1.303E-4*
	rinsed	*0.366*	*1.847*	*38981*	*1.308E-4*
S2	*original*	*0.511*	*1.745*	*72321*	*1.831E-4*
	rinsed	*0.512*	*1.741*	*72591*	*1.849E-4*
S3	*original*	*0.309*	*1.914*	*40988*	*5.756E-5*
	rinsed	*0.309*	*1.913*	*41148*	*5.664E-5*

3.3 Pore-network modelling

Pore-network modelling approach takes advantage of the analytical equations describing flow in capillary tubes. The computational domain of the pore space is simplified into an interconnected network of pores and throats (capillaries) that is equivalent to the original morphology of the pores. The extraction and subsequent Stokes flow simulation through the network was conducted in accordance with the procedure described within the documentation of the PoreSpy[22] and OpenPNM[23] frameworks. The comparison of the extracted pore network is depicted in Figure 5.

During flow simulation, constant pressure boundary conditions were set on the top and bottom planes of the sample, corresponding to the pressure difference of 10 Pa. After calculating the total flow, permeability was determined from the Darcy equation. The results of the computation were presented in Table 7.

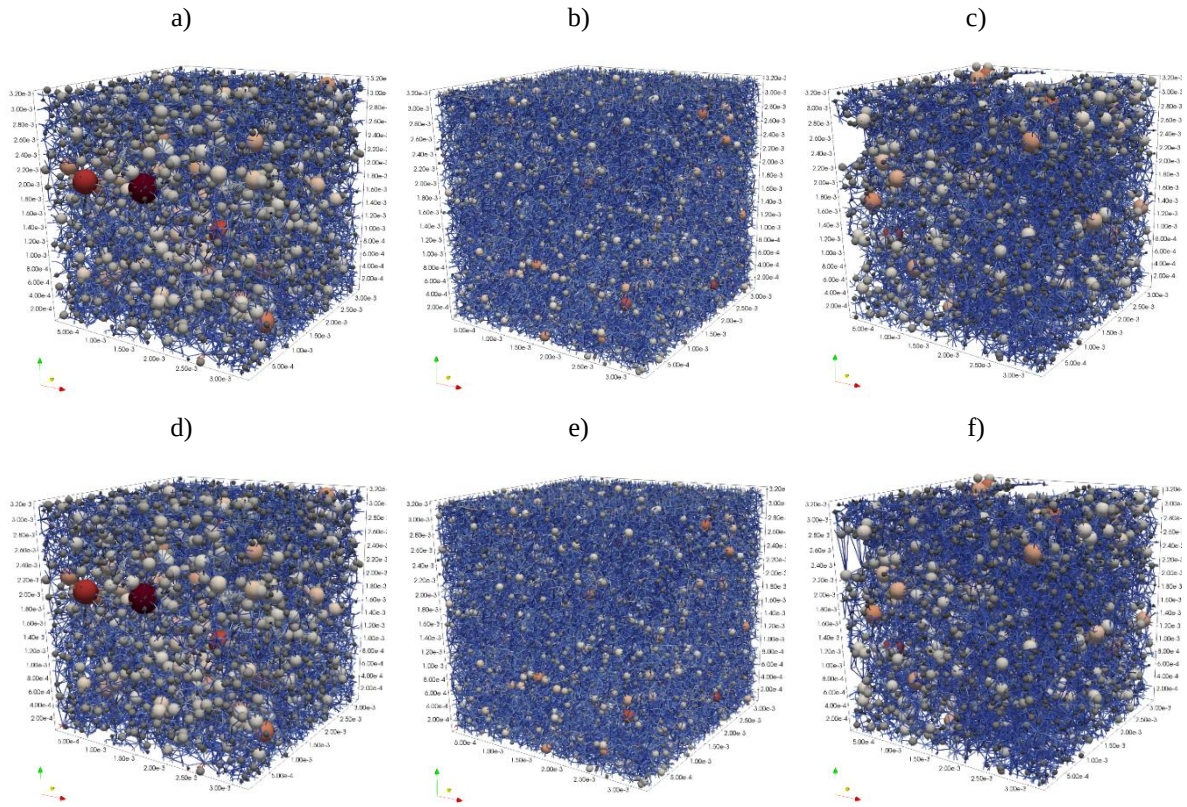

Figure 5 Comparison of pore networks obtained from PNM simulations for original samples: a) S1, b) S2, c) S3; samples after silt removal: d) S1, e) S2, f) S3

Table 7 Results of pore-network-based simulation

Sample		Permeability	Conductivity at 10°C
		$k[\mu m^2]$	$K_{10°C}$ [m/s]
S1	*original*	*23.644*	*1.786E-4*
	rinsed	*23.7626*	*1.787E-4*
S2	*original*	*28.407*	*2.136E-4*
	rinsed	*28.523*	*2.144E-4*
S3	*original*	*17.294*	*1.301E-4*
	rinsed	*17.361*	*1.305E-4*

3.4 Lattice-Boltzmann simulation

Lattice-Boltzmann method (LBM) is a computational fluid dynamics method especially well suited for direct flow simulations in porous media. Due to its lattice-based computational domain it is convenient for analyses on data retrieved from micro-CT scanning without the need of prior mesh creation. The solver used in the study was a multi-relaxation-time 3D LBM, using 19 velocity scheme implemented in TaichiLBM3D framework [24].

Constant pressure boundary conditions were used on inlet (top) and outlet (bottom) planes of the samples, with a pressure difference of 0.01 in lattice units (approximately 3.3 Pa pressure difference in SI-units) and periodic boundary conditions on the remaining planes. The simulations were conducted on a GPU for efficiency, as the LBM is both computationally expensive and well-suited for massive parallelization [25]. The resulting velocity and pressure fields of the flow through sample were combined with the Darcy equation, from which the permeability and hydraulic conductivity of the analyzed specimens were obtained. The streamline-depiction of flow was provided in Figure 6, while the outcomes of the procedure were summarized in Table 8

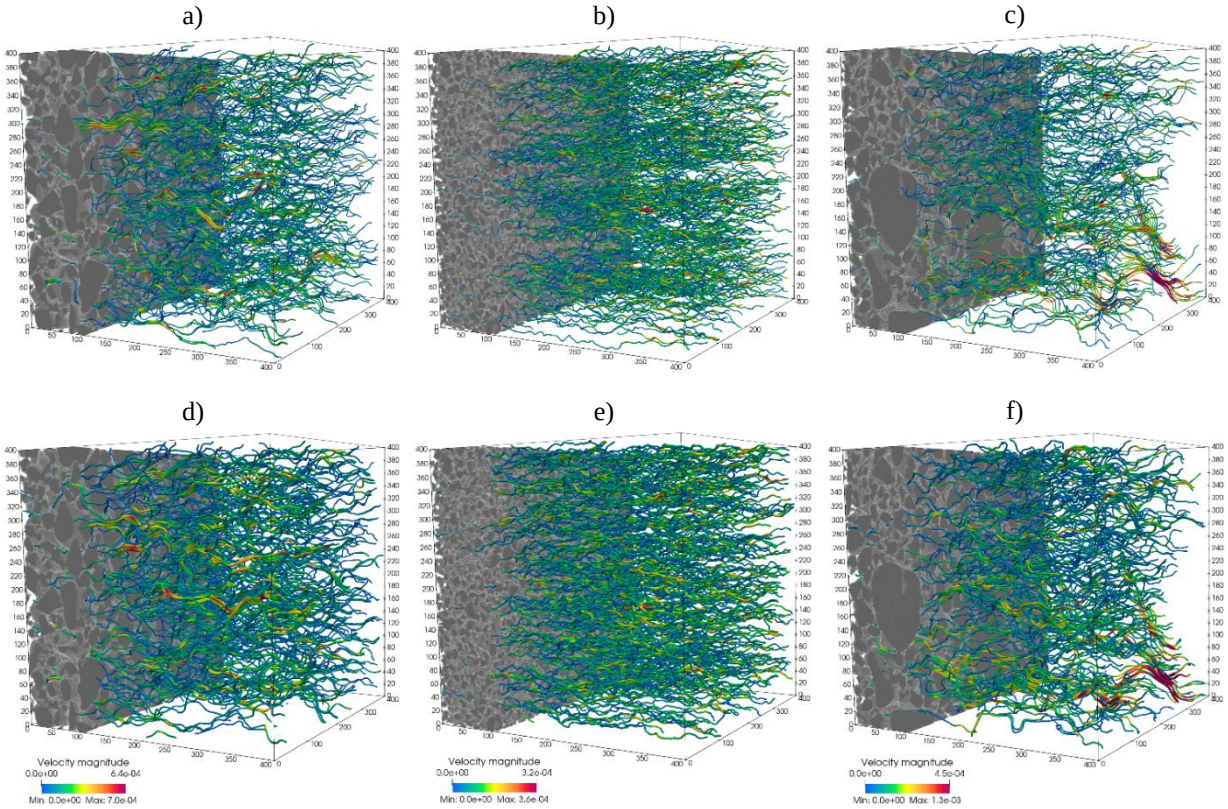

Figure 6 Streamlines obtained via LBM simulation in original samples: a) S1, b) S2, c) S3; samples after removal of the silt: d) S1, e) S2, f) S3; the axis corresponding to the flow direction in permeameter is rotated for clarity

IV. DISCUSSION ON METHODOLOGIES

The findings in the study back-up the general observation that the finest particles play the most crucial role in hydraulic properties of the soil [26]. As those particles fall in between larger grains, their morphology largely determines the properties of the pore channels. However, the influence is varied between presented approaches, as the image-based methods appear to be less influenced by the silt fraction than laboratory measurements. Its results are depicted in Fig. 7.

Table 8 Results of lattice-Boltzmann simulations

Sample		Permeability	Conductivity at 10°C
		$k[\mu m^2]$	$K_{10°C}[m/s]$
S1	*original*	*23.467*	*1.758E-4*
	rinsed	*25.370*	*1.904E-4*
S2	*original*	*20.903*	*1.565E-4*
	rinsed	*25.524*	*1.915E-4*
S3	*original*	*16.762*	*1.259E-4*
	rinsed	*18.751*	*1.407E-4*

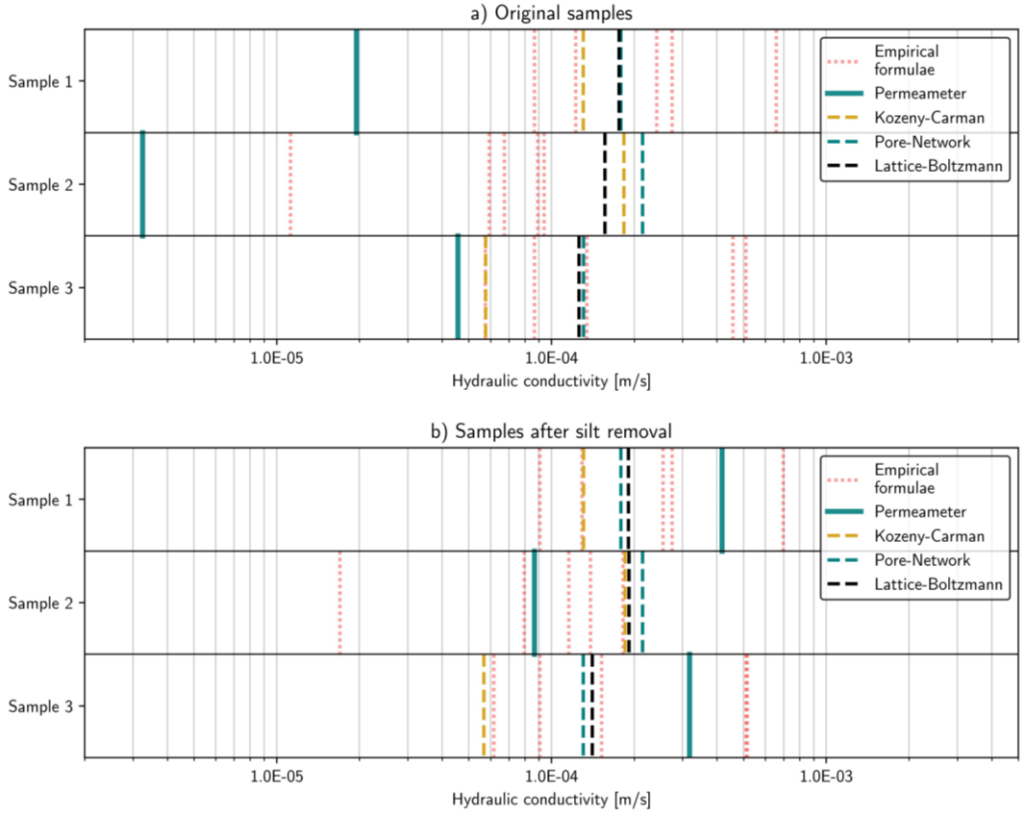

Figure 7 Summarized results of the methods presented in the study for: a) original and b) rinsed samples

Several factors contribute to that outcome. Firstly, fine particles may displace inside the sample during testing in permeameter, which may result in either clogging of the filter or the outlet pore channels. Such a behavior was observed during measurement of sample S2, as after reversal of the flow direction, some particles were observed suspended in the fluid inside the measurement pipe. Those migrating silt grains would become embedded in the filter fibers, effectively lowering its cross-sectional area and in result enlarging the resistance of the apparatus. This may explain the consecutive lowering of the measured conductivity values in the following trials. Such a behavior was not observed during testing of the samples with silt fraction removed or image-based methods, as the computational domain did not allow changes in the geometry induced by the drag forces of passing fluid.

Secondly, none of the employed image-based models took into account small-scale interactions at the interface between the fluid and soil particles, which influence would increase with the content of silt and clayey fraction. The highest rise in permeability was observed for sample S2 (almost 2 magnitudes) containing the largest amount of fine particles, while for coarser samples S1 and S3 the rise was moderate. Such an effect did not occur in micro-CT based methods, as the results remained fairly unchanged after the virtual removal of the silt.

Moreover, due to the intricacies in the methodology of scanning, reconstruction and binarization of the datasets, many particles constituting silt fraction were aggregated into bigger ones or not displayed at all considering applied resolution. This effectively reduced the number of grains under the removal threshold. As the minimal diameter for regions to be removed in the process approached closely to the resolution of the scans (63 μm in real sample corresponds approximately to the width of 8 voxels). Furthermore, it seems that micro-CT suits better for imaging sands with limited or none silt fraction. Eventually, for samples with noticeable amount of silt or clay the estimation of permeability will tend to be overestimated.

V. SUMMARY AND CONCLUSIONS

In this study, the influence of the silt fraction on the quality of permeability estimation was comprehensively assessed for sandy soils of diverse characteristics. Despite taking different approaches, both laboratory and image-based, the findings backed up the general view that the hydraulic properties of granular porous media are largely determined by the finest particles present in the composition.

As it emerges from the research, laboratory measurements were highly prone to the effects induced by the silt fraction, exhibiting up to two magnitudes of change after its removal. Even for samples containing below

1% of particles in question, the difference was significant. In contrast, image-based methods showed little sensitivity for all assessed sands. Results of Kozeny-Carman and pore-network approaches remained almost unchanged, while greater differences were observed for lattice-Boltzmann simulations. This was attributed to three main factors: possibility of colmatage, that was observed for the finest soil composition but unaccounted for in image-based models due to the stationary nature of the computational domain, lack or aggregation of finer particle representation in 3-D data caused by the limited resolution of the micro-CT scanning and disregarding of the effects at solid-fluid phase boundary in the employed methods and its implementation. While the last two may be overcome by using device with higher permitted resolution or more sophisticated numerical models, the clogging effects pose substantial difficulty in implementation within presented methods. The partial impacts of each of the aforementioned issues are yet to be determined.

Despite those observations, image-based methods provide a worthy alternative to conventional laboratory measurements, especially for coarser granular soils. They were able to provide a estimation closer to the values obtained from permeameter than widely-used correlative equations, reducing the uncertainties in the context of soil permeability. It is also worth noting that the extent of values resulting from assessed microstructure-based methods was significantly lower than those derived from empirical formulae.

Nevertheless, it is concluded that the approach to obtaining soil hydraulic properties should be focused on finding the upper and lower bounds rather than exact values of permeability, as this property still remains challenging for credible prediction. Given the methods presented and soil types under study, laboratory measurements may be used to evaluate the lower bound for permeability. Similarly, image-based assessment yielded slightly overestimated results, thus, suggesting the usage as the upper bound for sandy soils containing silt fraction. It may be speculated, that with the increase in coarseness of the composition, the discrepancies between laboratory and micro-CT based approaches should become consequently lower, and it will be covered in further research of the authors on this topic.

REFERENCES

[1] M. Kaviany, *Principles of Heat Transfer in Porous Media*. in Mechanical Engineering Series. (New York: Springer 1995). doi: 10.1007/978-1-4612-4254-3.

[2] A. E. Scheidegger, *The Physics of Flow Through Porous Media (3rd Edition)*. (Toronto: University of Toronto Press, 2020). doi: 10.3138/9781487583750.

[3] A. Verruijt, *Theory of Groundwater Flow*. (London: Macmillan Education UK, 1970). doi: 10.1007/978-1-349-00175-0.

[4] C. Cheng and X. Chen, "Evaluation of methods for determination of hydraulic properties in an aquifer–aquitard system hydrologically connected to a river," *Hydrogeol. J.*, vol. 15, no. 4, Jun. 2007, 669–678, doi: 10.1007/s10040-006-0135-z.

[5] P. Živković, M. Burečić Šafran, and B. Kovačević Zelić, "Comparison of measured and estimated permeability for artificially prepared coarse-grained soil samples," *Rud.-Geol.-Naft. Zb.*, vol. 36, no. 3, 2021, 167–178, doi: 10.17794/rgn.2021.3.12.

[6] F. Yu, D. Sun, M. Hu, and J. Wang, "Study on the pores characteristics and permeability simulation of pervious concrete based on 2D/3D CT images," *Constr. Build. Mater.*, vol. 200, Mar. 2019, 687–702, doi: 10.1016/j.conbuildmat.2018.12.135.

[7] L. Jiang *et al.*, "Permeability estimation of porous media by using an improved capillary bundle model based on micro-CT derived pore geometries," *Heat Mass Transf.*, vol. 53, no. 1, Jan. 2017, 49–58, doi: 10.1007/s00231-016-1795-4.

[8] S. Hamamoto, P. Moldrup, K. Kawamoto, T. Sakaki, T. Nishimura, and T. Komatsu, "Pore network structure linked by X-ray CT to particle characteristics and transport parameters," *Soils Found.*, vol. 56, no. 4, Aug. 2016, 676–690, doi: 10.1016/j.sandf.2016.07.008.

[9] J. Říha, L. Petrula, M. Hala, and Z. Alhasan, "Assessment of empirical formulae for determining the hydraulic conductivity of glass beads," *J. Hydrol. Hydromech.*, vol. 66, no. 3, Sep. 2018, 337–347, doi: 10.2478/johh-2018-0021.

[10] I. I. Sauerbrey, "On the Problem and Determination of the Permeability Coefficient," *Proc. VNIIG*, no. 3–5, 1932.

[11] F. Seelheim, "Methoden zur Bestimmung der Durchlässigkeit des Bodens," *Z. Für Anal. Chem.*, vol. 19, no. 1, Dec. 1880, 387–418, doi: 10.1007/BF01341054.

[12] A. Hazen, "XXIII. Some physical properties of sands and gravels, with special reference to their use in filtration," in *State Sanitation: A Review of the Work of the Massachusetts State Board of Health, Volume II*, Harvard University Press, 1917).

[13] W. Beyer, "Zur Bestimmung der Wasserdurchlässigkeit von Kiesen und Sanden aus der Kornverteilungskurve," *Wasserwirtsch. Wassertech.*, vol. 14, no. 6, 1964, 165–168.

[14] K. Urumović, S. Borović, K. Urumović, and D. Navratil, "Validity range and reliability of the United States Bureau of Reclamation (USBR) method in hydrogeological investigations," *Hydrogeol. J.*, vol. 28, no. 2, Mar. 2020, 625–636, doi: 10.1007/s10040-019-02080-2.

[15] L. A. Feldkamp, L. C. Davis, and J. W. Kress, "Practical cone-beam algorithm," *J. Opt. Soc. Am. A*, vol. 1, no. 6, Jun. 1984, 612, doi: 10.1364/JOSAA.1.000612.

[16] J. Kozeny, "Ueber kapillare Leitung des Wassers im Boden," *Sitzungsber Akad Wiss*, no. 136(2a), 1927, 271–306.

[17] P. C. Carman, *Flow of Gases through Porous Media*. (New York: Academic Press Inc., 1956).

[18] P. C. Carman, "Fluid Flow through Granular Beds.," *AIChE*, no. 15, 1937.

[19] F. A. L. Dullien, "Single-Phase Transport Phenomena in Porous Media," in *Porous Media* (Elsevier, 1979), 157–234. doi: 10.1016/B978-0-12-223650-1.50009-7.

[20] M. R. J. Wyllie and W. D. Rose, "Application of the Kozeny Equation to Consolidated Porous Media," *Nature*, vol. 165, no. 4207, Jun. 1950, 972–972, doi: 10.1038/165972a0.

[21] T. G. Tranter, M. D. R. Kok, M. Lam, and J. Gostick, "pytrax: A simple and efficient random walk implementation for calculating the directional tortuosity of images," *SoftwareX*, vol. 10, Jul. 2019, 100277, doi: 10.1016/j.softx.2019.100277.
[22] J. Gostick *et al.*, "PoreSpy: A Python Toolkit for Quantitative Analysis of Porous Media Images," *J. Open Source Softw.*, vol. 4, no. 37, May 2019, 1296, doi: 10.21105/joss.01296.
[23] J. Gostick *et al.*, "OpenPNM: A Pore Network Modeling Package," *Comput. Sci. Eng.*, vol. 18, no. 4, Jul. 2016, 60–74, doi: 10.1109/MCSE.2016.49.
[24] J. Yang, Y. Xu, and L. Yang, "Taichi-LBM3D: A Single-Phase and Multiphase Lattice Boltzmann Solver on Cross-Platform Multicore CPU/GPUs," *Fluids*, vol. 7, no. 8, Aug. 2022, Art. no. 8, doi: 10.3390/fluids7080270.
[25] A. M. Bruaset and A. Tveito, Eds., *Numerical solution of partial differential equations on parallel computers*. in Lecture notes in computational science and engineering, no. 51. (Berlin: Springer, 2006).
[26] K. Terzaghi, R. B. Peck, and G. Mesri, *Soil mechanics in engineering practice. Third edition.* (New York: John Wiley 1995).